Faraday Discussions

Accepted Manuscript

This manuscript will be presented and discussed at a forthcoming Faraday Discussion meeting. All delegates can contribute to the discussion which will be included in the final volume.

Register now to attend! Full details of all upcoming meetings: http://rsc.li/fd-upcoming-meetings

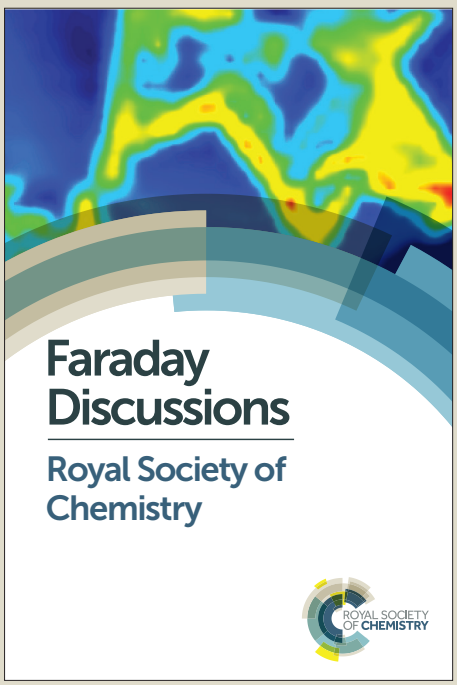

This is an *Accepted Manuscript*, which has been through the Royal Society of Chemistry peer review process and has been accepted for publication.

Accepted Manuscripts are published online shortly after acceptance, before technical editing, formatting and proof reading. Using this free service, authors can make their results available to the community, in citable form, before we publish the edited article. We will replace this *Accepted Manuscript* with the edited and formatted *Advance Article* as soon as it is available.

You can find more information about *Accepted Manuscripts* in the Information for Authors.

Please note that technical editing may introduce minor changes to the text and/or graphics, which may alter content. The journal's standard Terms & Conditions and the Ethical guidelines still apply. In no event shall the Royal Society of Chemistry be held responsible for any errors or omissions in this *Accepted Manuscript* or any consequences arising from the use of any information it contains.

ROYAL SOCIETY OF CHEMISTRY

www.rsc.org/faraday_d

Journal Name

RSCPublishing

ARTICLE

Amorphous calcium phosphate phase mediated crystal nucleation kinetics and pathway

Cite this: DOI: 10.1039/x0xx00000x

Shuqin Jiang,[a,b] Haihua Pan,[*a] Yan Chen,[b] Xurong Xu[b] and Ruikang Tang[a,b]

Received 00th January 2012,
Accepted 00th January 2012

DOI: 10.1039/x0xx00000x

www.rsc.org/

Generally, solution nucleation model is used to study the biomineralization kinetics. However, we found that the amorphous calcium phosphate (ACP) mediated hydroxyapatite (HAP) nucleation in simulated body fluids (SBF) had the different profile from the linear relationship between ln$J$ and ln^{-2}S (J, nucleation rate; S, supersaturation). This behaviour was alternatively explained by a developed heterogeneous nucleation theory, which indicated that HAP was nucleated at the ACP-solution interface via a polymorph transformation. Based upon this new model, we demonstrated experimentally that the embedded polymer molecules inside ACP were inert on HAP nucleation kinetics; rather, the polymers adsorbed on ACP surface could inhabit HAP nucleation from ACP. It further confirmed the heterogeneous nucleation pathway of HAP on the precursor phase. The present study would provide an in-depth understanding about HAP formation for ACP-mediated crystallization.

Introduction

Formation of biominerals is believed to be controlled by the principle of crystallization. During typical crystallization process, nucleation is the first step but it determines crystal phase, size and orientation.[1] Among the inorganic crystal materials, hydroxyapatite (HAP, $Ca_5(PO_4)_3OH$) has attracted much attentions because it is the main component of biological bones and teeth.[2] As a sparingly soluble mineral phase, HAP is actually highly supersaturated in simulated body fluids (SBF)[3] but its direct nucleation from solution is well inhibited *in vivo*. It has been evidenced that amorphous calcium phosphate (ACP) phase is the intermediate phase for HAP crystallization in both hard tissue formation (*in vivo*) and biomimetic mineralization (*in vitro*).[4] Recently, the ACP-mediated HAP crystallization rather than direct HAP crystallization has been accepted as the biomineralization pathway in living organisms.[4c] This non-classical pathway exhibits different behaviour from the conventional understanding for solution crystallization. For example, in a previous work we observed an unexpected faster crystallization of HAP at lower pH (means lower supersaturation) in ACP-mediated HAP crystallization.[5] These nucleation data cannot be explained by the established linear relationship between lnJ_N (J_N for nucleation rate) and ln^{-2}S (S for supersaturation) (J-S relationship), in which lower supersaturation should result in slower nucleation. It is interesting to learn whether this abnormal profile is valid in a broad spectrum of calcium phosphate solution that closes to physiological fluid. In this work, we examined the nucleation kinetics over a variety of pH, supersaturation and temperature conditions in the absence and presence of polymers. The experimental results suggested that HAP was always nucleated at the ACP-solution interface via a polymorph transformation. It was also demonstrated that the solution species were greatly altered in the presence of ACP precursor phase and thereby, the direct use of supersaturation respective to HAP for the kinetic discussion became inappropriate. We suggested a developed heterogeneous nucleation model, which highlighted the ACP-solution interaction in the kinetic controls of HAP nucleation.

Experiments

Materials

Polyacrylate (PAA, Mw=2.1kD, Sigma-Aldrich, USA), poly-Aspartate (p-Asp, Mw=27kD, Alamanda Polymers, USA) and poly-Glutamate (p-Glu, Mw=2-15kD, GL Biochem Ltd, Shanghai, China). All other chemicals were analytical grade and purchased from Aladdin Reagent (Shanghai, China) unless specially described. The solutions were filtered through 0.22 μm Millipore membranes prior to use.

HAP Crystallization

Calcium solutions (Ca) contained $CaCl_2$ and $MgCl_2$. Phosphate solutions (P) contained Na_2HPO_4, Na_2SO_4, NaCl, KCl, N-2-hydroxyethylpiperazine-N'-2-ethane sulfonic acid (HEPES, GenomBioMed Technology Inc., Hangzhou, China). SBF solutions were prepared by a rapid mixing of the equal volumes of Ca and P solutions with designated concentrations, and solution compositions were close to body fluid (Tables S1 in ESI†). After the mixing, the pH curve of the reaction solution was monitored by a PHSJ-3F pH meter with E-201-C

composite electrode (Leici Instrument, Shanghai, China). The induction time, t_i, for HAP nucleation was determined by the abrupt change in pH curves as described in a previous work.[6] Since ACP were formed immediately (within few seconds) after the mixing, the induction time for ACP nucleation were not investigated in the current work. Each experiment was repeated at least for four times and the relative standard deviations for induction time were around 8%, which were marked as the error bars in the plots. The typical reproducibility of pH curves was shown in Fig. S1 in ESI†.

Polymer additives

PAA, p-Asp, and p-Glu were used as prototypes for non-collagenous proteins (NCPs) in biomineralization. There were two protocols for the introduction of polymer additives (stock solution: 10 mg ml^{-1}) into the mineralization reaction: (i) pre-mixing: 20 μl was added into 5 ml of P solution prior to mixing with 5 ml Ca. (As explained later, in this protocol the polymer molecules were mainly embedded inside the resulted ACP). (ii) post-mixing: 20 μl polymer stock solution was added into the ACP suspension after the mixing of 5 ml P and 5 ml Ca for 10 min (as explained later, the polymer molecules were mainly absorbed on the ACP surface). All the experiments were conducted at 37.0±0.5°C, pH=7.4 ± 0.02, and the finial concentration of the polymer additive was 20 μg ml^{-1} (solution compositions were listed in Table S2 in ESI†).

Characterizations

During the reaction, 10 ml suspension was withdrawn and centrifuged at 10,000 g for 2 min (Luxian, GL-22M, China), and washed with ethanol. The obtained mineral phase was characterized by FITR (Shimadzu Iraffinity-1) and X-ray diffraction (XRD, Rigaku D/MAX-2550pc, Cu Kα radiation λ=1.54 Å). For TEM/SAED (Hitachi HT-7700 or JEOL 2100F) examination, the specimens were obtained by paddling copper grid in suspension, and washing with water and ethanol, and lamp-light dried. The zeta potentials of precipitate were determined by Zetasizer Nano S (Malvern).

The calcium and phosphate concentrations in the solution were measured using ICP-AES (Thermo Fisher iCAP 6300). For this purpose, aliquots were taken from the supernatant solution periodically, filtered with a syringe filter with a pore size of 25 nm to remove the ACP precipitates, and then immediately diluted with 5% hydrochloric acid.

Solution Chemistry Calculation

The supersaturations of the solutions were calculated by VMINTEQ 3.0.[7a] Davies approximation of the Debye–Hückel equation was used for calculating the activity coefficients (parameter b = 0.3 is applied). The solubility product, K_{SP}, of HAP (p*K*sp = 58.33, MINTEQ database: NIST 46.7), and ACP (p*K*sp= 25.5[7b,7c]) were used in calculation.

***J-S* relationship:**

In classical nucleation kinetics, the nucleation rate J_N is given as[8]

$$J_N = K_1 \exp\left[\frac{-16\pi\gamma^3\Omega^2}{3(k_BT)^3(\ln S)^2}\right] = K_1 \exp[\frac{K_2}{(\ln S)^2}] \quad (1)$$

where K_1, pre-exponential factor; k_B, the Boltzmann constant; T, the absolute temperature; γ, the interfacial energy between the crystals and the mother phase; Ω, the volume of the growth units. S, the supersaturation. Eq. (1) shows the curve of $\ln J_N$ vs $\ln^{-2}S$ should exhibit a linear relationship.

The supersaturation with respect to HAP and ACP is written as S_{HAP}, and S_{ACP} respectively, which is given by,

$$S_{HAP} = \frac{\{Ca^{2+}\}^5\{PO_4^{3-}\}^3\{OH^-\}}{K_{sp,HAP}} \quad (2)$$

$$S_{ACP} = \frac{\{Ca^{2+}\}^3\{PO_4^{3-}\}^2}{K_{sp,ACP}} \quad (3)$$

Where $\{X\}$, is the activity of species X and $K_{sp,X}$ is the solubility product of X. To measure the nucleation rate, one of the most common ways is to measure the induction time of nucleation at different supersaturations. In practices, J_N is also defined as,[8]

$$J_N = 1/(t_i V) \quad (4)$$

in which V is the volume of the system, t_i is the induction time.

Results and Discussion

Nucleation Kinetics

Gnereally, crystal nucleation from solutions should obey the linear *J-S* relationship between $\ln J_N$ and $\ln^{-2}S$. However, such a relationship was not found in the current study of HAP nucleation in SBF. There were two different liner regions in the plot of $\ln J_N$-$\ln^{-2}S$ in the current study (Fig. 1a). At first glance, this kind of bimodal nucleation profile had been reported as the transition from homogeneous nucleation to heterogeneous nucleation[9] or from structural matched nucleation to structural mismatched heterogeneous nucleation.[10] However, in both cases, a smaller slope (low nucleation rate) should be expected in the lower supersaturation region, which was in contradicted with the observed data in our experiments (Fig. 1b). This unexpected phenomenon could be observed over a broad spectrum of calcium phosphate solutions at varies temperature (Fig. 2a) and pH (Fig. 2b) in our studies. However, the previously established *J-S* relationship could not explain this HAP nucleation kinetic profile in SBF.

ACP-mediated Crystallization Pathway

The crystallization of HAP in SBF is monitored by solution pH drop (Fig. 3a). Typically, the pH curve can be divided into three different stages: I, induction period; II, HAP crystallization stage; III, post crystallization stage.[5,6] The mineral phase at each stage was *ex-situ* characterized by FTIR (Fig. 3b), XRD (Fig. 3c) and TEM (Fig. 3d-f). For the conventional understanding, the supersaturated solution is in a metastable state and there is no solid precipitation in the induction period (Stage I). Actually, we noted that the precursor

solid phase, ACP, was already precipitated in this stage. The formation and growth or ripening of ACP particles was observed (cf. Fig. 3d, Fig. S2 in ESI†) at large scale. The broad FTIR absorption bands around 1055 cm^{-1} (phosphate ν_3 vibrations) and 570 cm^{-1} (phosphate ν_4 bending) indicated the amorphous state of calcium phosphate. The ACP phase was also confirmed by the broad XRD diffraction at about 30° (2θ). The splitting of phosphate ν_3 vibration and ν_4 bending absorption bands in FTIR (Fig. 3b), and the appearance of sharp XRD diffractions indicated the formation HAP (Fig. 3c) at stage II. Under TEM, the newly formed platelet-like crystallites were mainly on the existed ACP aggregates (Fig. 3e). It followed heterogeneous nucleation behaviour of the crystallites on the precursors (Fig. 3f). The electron diffraction patterns showed that the crystallites were HAP (Fig. 3e inset). For the specimens collected at the phase transition period (at induction time point in the pH curve, cf. Fig. 3a), the out-growth of platelet-like nuclei on the ACP surface was frequently observed (Fig. 3g-i). These evidences provided the scenario of ACP-mediated crystallization pathway: 1) a primary formation of ACP; 2) polymorphic transformation to HAP at ACP-solution interface.

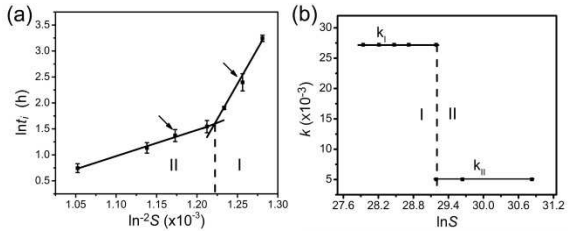

Fig. 1 (a) Plot of Int_i vs $ln^{-2}S$ for HAP nucleation at 25°C, pH=7.4. The nucleation kinetics can be divided into two regions, named I and II respectively. Solutions and precipitation used for further characterization were indicated by arrows. (b) The slope is higher for low supersaturation.

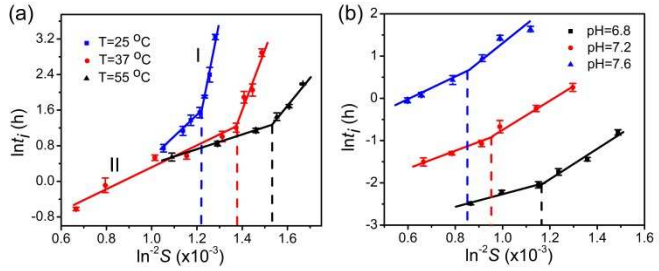

Fig. 2 plot of Int_i vs $ln^{-2}S$ for ACP mediated HAP nucleation at different temperature (a) and pH (b).

Accordingly, the nucleation kinetics data could be divided into two regions (I, II in Fig. 1b). Previously, Eanes *et al.* suggested two types of ACP, which were called as discoidal-ACP and spheroidal-ACP.[7d] Therefore, it might be reasonable that the two kinds nucleation behaviours were attributed to the formation of different types of ACP in the experiment system. However, no significant difference between the resulted ACP in these two regions was detected by using FTIR (Fig. 4a), XRD (Fig. 4b), and TEM (Fig. 4c-f). In addition, ICP-AES study showed that the Ca/P ratios of the resulted ACP were 1.54 ± 0.05 and 1.54 ± 0.04 in the region of I and II (cf. Fig. 1a), respectively. We also examined their solubility products, pK_{sp}, which were 25.87±0.04 and 25.96 ± 0.08 for the ACP samples obtained from the regions I and II, respectively (see Table S3 and S4 in ESI†). Moreover, the zeta potentials of these ACPs were also exactly the same (cf. Fig. S3). In fact, all applied characterization methods could not distinguish one ACP from the other for these regions. As the morphology of these ACP particles was always spherule (Fig. 4c, 4e) without any change, we concluded that the ACP phases formed at region-I and II were spheroidal-ACP and they were the same.[7b,7d,11] Accordingly, the different nucleation behaviours for region-I and II was not caused by the formation of different types of ACP.

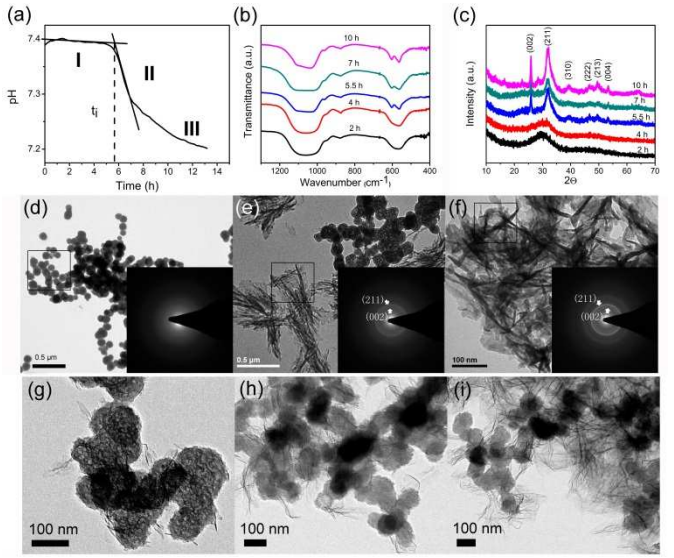

Fig. 3 Crystal nucleation kinetics and crystallization pathway. (a) The representative pH curve of calcium phosphate solutions (lnS=28.47, pH=7.4,T=25°C, Table S1 for details). The crystallization processes could be divided into three stages. I, induction period; II, crystallization stage; III, post crystallization stage. The FTIR spectra (b) and XRD patterns (c) of precipitations at stage I, II and III repectively. 2h and 4h, ACP; 5.5h and 7h, weak crystallized HAP; 10h, crystallized HAP. (d-f) TEM images and SAED patterns (inset) show typical morphology and phase of (d) stage I (ACP) , (e) II (ACP, HAP) and (f) III (HAP), respectively. (g-i) TEM images of mineral at the induction period (5.5 h).

ACP-mediated HAP Nucleation Kinetics

Since the HAP was precipitated via ACP-mediated pathway. The direct nucleation of HAP from solutions is not valid in the kinetic discussion. Previously, we have developed a heterogeneous nucleation model for ACP-mediated HAP nucleation, and the nucleation rate of HAP, $J_{N,hetero}$, is given as,[5]

$$J_{N,hetero} = K \cdot C_{ACP} \{Ca\}_{eff}^2 \quad (5)$$

$$K = K_1 \exp(\frac{-\Delta G^*_{react}}{k_B T}) \exp(\frac{-\Delta G^*_{nucl,hetero}}{k_B T}) f \quad (6)$$

$$\ln J_{N,hetero} = \ln C_{ACP} \{Ca\}_{eff}^2 - [\frac{\Delta G^*_{react} + \Delta G^*_{\mathrm{nucl,hetero}}}{k_B T} - \ln K_2] \quad (7)$$

$$K_2 = K_1 f \quad (8)$$

where, K_1 is the pre-exponential factor; ΔG^*_{react}, the chemical reaction barrier for the incorporation of free calcium into HAP nuclei; $\Delta G^*_{nucl,\ hetero}$, the nucleation barrier for heterogeneous nucleation of HAP from ACP; f, the converting factor from surface area to the amount of ACP (ie. $A_{particles} = fC_{ACP}$). C_{ACP}, the amount of ACP formed; $\{Ca\}_{eff}$, the effective activity of calcium ions (after the precipitation of ACP). Due to the precipitation of ACP, all solutions become saturated with ACP in spite of their different supersaturations at the original solution states. Therefore, K could be treated as a constant in the ACP mediated HAP crystallizaiotn. Thus, there should be a linear relationship between $\ln J_{N,hetero}$ and $\ln(\{Ca\}_{eff}^2 C_{ACP})$ (cf. eq. 7; the slope was fixed as 1.0 according to eq. 5; C_{ACP} was obtained by solution chemistry calculation, see Tables S1 and S5 in ESI† for the details) and it was named as *J-C* relationship. We found that this nucleation rule could be used to fit the nucleation kinetics well for a wide spectrum of calcium phosphate solutions even at different temperature (Fig. 5a) and pH (Fig. 5b).

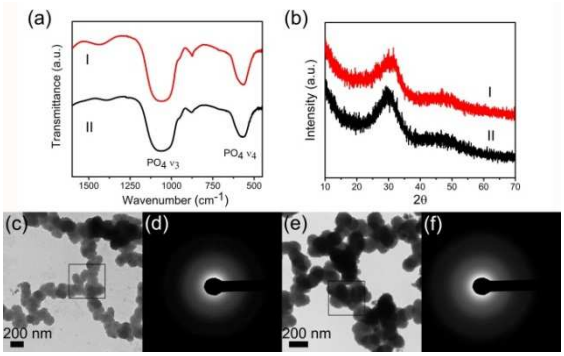

Fig. 4 Characterizations of ACP in region I and II (see Fig. 1) (a) FTIR spectra, (b) XRD patterns, (c, e) TEM images and (d,f) SAED patterns. There was no obvious difference between these ACPs.

Eq. 7 shows that the nucleation barriers ($\Delta G^*_{react}+\Delta G^*_{nucl,hetero}$) are correlated to the intercept of *J-C* relationship. By measuring the intercepts of *J-C* curves at different temperatures, the values of $\Delta G^*_{react}+\Delta G^*_{nucl,hetero}$ could be estimated. In our experiments, the energy of $\Delta G^*_{react}+\Delta G^*_{nucl,hetero}$ was about 13.6 k_BT (cf. Fig. 6), which was much smaller than that of direct HAP nucleation from the solution, which was >150 k_BT [10b,12]. It followed that the nucleation barrier of ACP mediated HAP crystallization pathway was ten-fold lower than its direct nucleation from solutions. Therefore, the former pathway might be more preferred for HAP formation in SBF solutions.

Free Calcium Ion and HAP Nucleation

In the ACP-mediated formation pathway, the polymorphic transformation from ACP to HAP is the key to generate HAP. Stoichiometrically, the Ca/P ratio of ACP precursor (1.5) is less than that of HAP crystallites (1.67). So, during the polymorphic transformation of ACP to HAP, additional calcium ions should be required from solution as the following chemical equation:

$$3Ca_3(PO_4)_2 + Ca^{2+} + 2H_2O \rightarrow 2Ca_5(PO_4)_3OH + 2H^+ \quad (9)$$

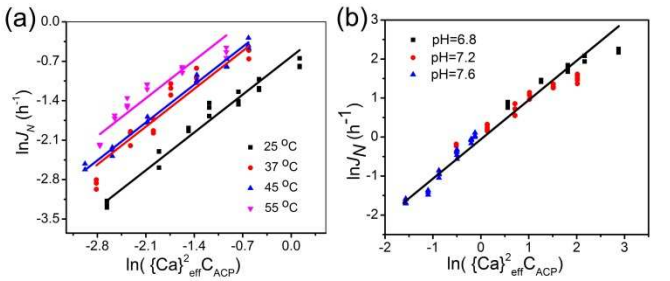

Fig. 5 Nucleation rate $\ln J_N$ (h^{-1}) vs $\ln(\{Ca\}_{eff}^2 C_{ACP})$ for calcium phosphate solutions at different (a) temperature and (b) pH. All kinetics data obey *J-C* relationship.

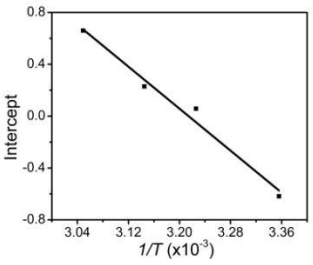

Fig. 6 Plot of Intercepts of J-C relationship vs 1/T. The slope of this plot is the nucleation barrier (cf. Eq. 7).

According to Eq. 7, the nucleation rate of HAP from ACP precursor should be dependent on the effective activity of calcium and the amount of ACP. With the increasing of initial solution supersaturation, more ACP would be precipitated (cf. Table S5) in the system but the change of the effective activity of calcium was ignorable (cf. Table S5) because all solutions became saturated with ACP. This followed that the effective activity of calcium was not sensitive to the change of initial (apparent) supersaturation (cf. Table S5) when pH and temperature were fixed. However, we found that the effective calcium activity was relevant to the solution pH (Table S6). In the solution, $\{PO_4\}$ was extremely sensitive to pH due to the association and disassociation balance, $\{Ca\}$ could be also in turn affected by pH due to the constant of the activity product of $\{Ca\}^3\{PO_4\}^2$ in the system. In order to exclude the effect from different ACP amount, we examined the HAP nucleation kinetics in the solutions with the fixed amount of ACP (C_{ACP}=1.648 mM). By slight decreasing solution pH from 7.6 to 6.8 (Table S6), HAP always nucleated faster at higher level of $\{Ca\}_{eff}$ (Fig. 7). This supported that the reaction of free calcium ion in solution with ACP was a key factor to control the heterogeneous nucleation of HAP.

Polymer Additives and Nucleation Kinetics

In biomineralization and biomimetic mineralization, organic additives play paramount roles in the crystallization regulations. The inhibitory effect of PAA on crystallization has been widely reported.[13] However, in this work we found that the inhibition is highly depended upon the protocols for the introduction of PAA. When the small amount of PAA (20 μg/ml was

introduced before the formation of ACP (pre-mixing protocol), there was no obvious inhibiting effect for HAP nucleation (Fig. 8a). But, if the addition of PAA occurred after the formation of ACP (post-mixing protocol), the induction time of HAP nucleation was significantly prolonged. It demonstrated the strong inhibition effect of the later added PAA. Similar profile was also found in the case of p-Asp and p-Glu (Fig. S4). It was interesting to note that TEM observations did not find any obvious change on the morphology and size of ACP by using the different protocols (cf. Fig. S5). As the compositions for both protocols were exact the same, $\{Ca\}_{eff}^2 C_{ACP}$ should be the same as well (the effect of 20 μg/ml PAA on the free calcium concentration reduction was ignorable). By using Eq. 5 and the ACP-mediated crystallization, the factor K should be affected by PAA. It implied that the chemical process for the interaction of free calcium ion with ACP surface would be affected. We assumed that in the pre-mixing protocol, PAA molecules were mainly embedded inside ACP; in post-mixing protocols, PAA were adsorbed on ACP surface (Schemed Fig. 8d). Thus, ACP-solution interface was almost the same as that of the control experiment (without PAA) using the pre-mixing protocol. Therefore, the introduction of PAA additive could not affect the HAP nucleation rate on ACP. But for the post-mixing protocol, the adsorbed PAA might affect the direct reaction between the free calcium and ACP, and subsequently inhibit HAP nucleation. This phenomenon would provide an alternative novel pathway to control HAP nucleation in addition to ACP amount or free calcium concentration.

The further characterizations of ACP particles revealed the possible locations of PAA. Firstly, FTIR spectra indicated the presence of PAA for ACP particles obtained by both protocols. The appearance of additional bands around 1565 and 1408 cm^{-1} (for the anti-symmetrical and symmetrical vibrations of the carboxyl group for PAA) supported the co-precipitation of PAA with ACP (Fig. 8b). Secondly, distinct zeta potential value has been observed for ACP particles by using the different protocols (Fig. 8c). Zeta potential of ACP particles in pre-mixing protocol (-1.12 ± 0.08 mV; mean ± s.d., n=5) was close to that of control (3.34 ± 0.22 mV, n=5). It followed that the PAA molecules were almost embedded inside ACP particles. In contrast, in the case of post-mixing, the zeta potential of ACP became highly negative (-11.70 ± 0.39 mV, n=5), implying the adsorption of the negatively charged PAA on the ACP surface.

Conclusions

It has been demonstrated that the well-established J-S relationship for solution nucleation cannot be used to match the ACP-mediated HAP nucleation kinetics. In the presence of the ACP precursor phase, HAP is heterogeneously nucleated at the ACP-solution interface via a polymorph transformation. Accordingly, ACP phase and free calcium ions (Fig. 8d) are the keys to control the nucleation kinetics of HAP from ACP. By using polymers, it further confirms that the protocols of mineralization experiments can also affect HAP nucleation in the ACP-mediated crystallization. This work provides an alternative kinetic understanding about HAP formation under physiological condition and highlights the phase transition pathway by using developed heterogeneous nucleation model.

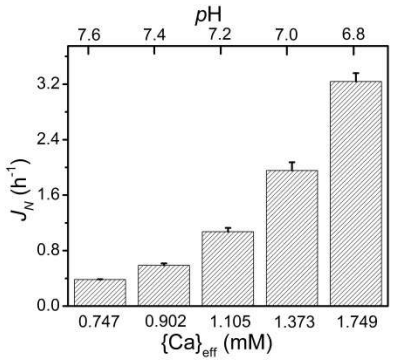

Fig. 7 Polt of J_N (h^{-1}) vs $\{Ca\}_{eff}$ (mM) at 37°C with fixed C_{ACP} (1.648 mM, relative error is less then ± 0.8%), and $\{Ca\}_{eff}$ was sensitive to the changing of pH. The nucleation rate was increased as the increasing of $\{Ca\}_{eff}$.

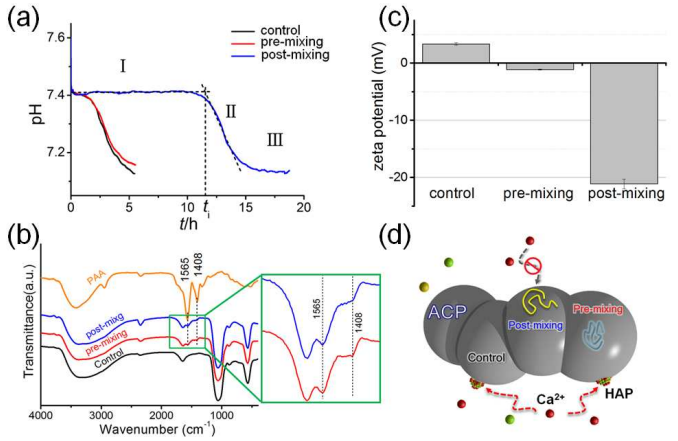

Fig. 8 (a) Representative pH curves of HAP crystallization in the presence (pre-mixing and post-mixing) and absence (control) of PAA. (b) FTIR spectra and (c) zeta potentials of precipitates in different protocols at 10 min. (d) The scheme of ACP-mediated HAP crystallization.

Acknowledgements

We thank James J. De Yoreo for helpful discussions. This work was supported by the Fundamental Research Funds for the Central Universities, National Natural Science Foundation of China (91127003)

Notes and references

[a] Centre for Biomaterials & Biopathways, and Department of Chemistry, Zhejiang University, Hangzhou, Zhejiang 310027, China. E-mail: rtang@zju.edu.cn

[b] Qiushi Academy for Advanced Studies, Zhejiang University, Hangzhou, Zhejiang 310027, China. E-mail: panhh@zju.edu.cn

†Electronic Supplementary Information (ESI) available: Solution compositions, Figures and Tables. See DOI: 10.1039/b000000x/

1 F. C. Meldrum and H. Cölfen, *Chem. Rev.*, 2008, **108**, 4332.

2 (a) E. Beniash. *Wiley Interdiscip. Rev.: Nanomed Nanobiotechnol.*, 2011, **3**, 47; (b) R. Z. Legeros. *Adv. Dent. Res.* 1988, **2**, 164.

3 (a) A. Oyane, H. M. Kim, T. Furuya, T. Koukubo, T. Miyazaki and T. Nakamura, *J. Biomed. Mater. Res., Part A*, 2003, **65**, 188; (b) T. Kokubo and H. Takadama, *Biomaterials*, 2006, **27**, 2907.

4 (a) J. D. Termine and A. S. Posner. *Calcif. Tissue Res.,* 1967, **1**, 8; (b) A. L. Boskey. *J. Dent. Res.,* 1997, **76**, 1433; (c) J. Mahamid, B. Aichmayer and E. Shimoni, et al. *Proc. Natl. Acad. Sci. U. S. A.*, 2010, **107**, 6316; (d) L. B. Gower, *Chem. Rev.,* 2008, **108**, 4551.

5 S. Jiang, Y. Chen and H. Pan, *Phys. Chem. Chem. Phys.*, 2013, **15**, 12530.

6 (a) Y. Chen, W. Gu, H. Pan, S. Jiang and R. Tang, *CrystEngComm*, 2014, **16**, 1864; (b) P. B. Y. Ofir, R. G. Lippman, N. Garti and H. Füredi-Milhofer, *Cryst. Growth Des.*, 2003, **4**, 177; (c) X. Yang, B. Xie, L. Wang, Y. Qin, Z. J. Henneman and G. H. Nancollas, *CrystEngComm*, 2011, **13**, 1153; (d) B. Xie, T. J. Halter, B. M. Borah and G. H. Nancollas, *Cryst. Growth Des.*, 2014, **14**, 1659.

7 (a) J. P. Gustafsson, 2010. Visual MINTEQ, Version 3.0, Stockholm. Available from http://www.lwr.kth.se./English/OurSoftware/vminteq. (b) M. R. Christoffersen, J. Christoffersen, W. Kibalczyc, *J. Cryst. Growth,* 1990, **106**, 349; (c) S. V. Dorozhkin and M. Epple, *Angew. Chem. Int. Ed.,* 2002, **41**, 3130; (d) E. D. Eanes, J. D. Termine and M. U. Nylen, *Calcif. Tissue Int.*, 1973, **12**, 143.

8 X. Y. Liu and K. Sato, *In Advances in crystal Growth Research, Elsevier,* Amsterdam, 2001, 42.

9 (a) O. Söhnel and J. M. Mullin, *J. Cryst. Growth*, 1978, **44**, 377; (b) J. M. Mullin and H. M. Ang, *Faraday Discuss. Chem. Soc.,* 1976, **61**, 141.

10 (a) X. Y. Liu and S. W. Lim, *J. Am. Chem. Soc.,* 2002, **125**, 888; (b) H. Jiang, X.Y. Liu, G. Zhang and Y. Li, *J. Biol. Chem.*, 2005, **280**, 42061.

11 (a) C. Combes and C. Rey, *Acta Biomater.*, 2010, **6**, 3362; (b) S. V. Dorozhkin, *Acta Biomater.*, 2010, **6**, 4457.

12 W. J. E. M. Habraken, J. Tao and L. J. Brylka, et al, *Nat. Commun.*, 2013, **4**, 1507.

13 (a) S. Schweizer and A. Taubert, *Macromol. Biosci.*, 2007, **7**, 1085; (b) Z. Amjad, *Langmuir*, 1989, **5**, 1222; (c) A. Bigi, E. Boanini, G. Cojazzi, G. Falini and S. Panzavolta, *Cryst. Growth Des.,* 2001, **1**, 239; (d) V. Ball, M. Michel, F. Boulmedais, J. Hemmerle, Y. Hailel, P. Schaaf and J. C. Voegel, *Cryst. Growth Des.*, 2006, **6**, 327.

